

Thickness-Controlled Synthesis of Ultrathin Au Sheets and Surface Plasmonic Property

Hai Li Qin,^{†,§} Dong Wang,^{†,§} Zeng Li Huang,[†] Dong Min Wu,[†] Zhi Cong Zeng,[‡] Bin Ren,[‡] Ke Xu,[†] and Jian Jin^{*,†}

[†]*i-LAB* and Nano-Bionics Division, Suzhou Institute of Nano-Tech and Nano-Bionics, Chinese Academy of Sciences, Suzhou 215123, China

[‡]State Key Laboratory of Physical Chemistry of Solid Surfaces and Key Laboratory of Analytical Sciences, College of Chemistry and Chemical Engineering, Xiamen University, Xiamen 361005, China

S Supporting Information

ABSTRACT: Thickness-controlled synthesis of nanosheets of nonlayered materials is of scientific significance yet greatly underdeveloped because of the lack of controllable means of inducing anisotropic growth of 2D structures. Here we report a novel 2D template-directed synthesis of ultrathin single-crystalline Au nanosheets with well-tuned thicknesses of several to tens of nanometers, large areas (>100 μm^2), and atomically flat surfaces. The 2D template is composed of hundred-nanometer-thick water layers sandwiched by lamellar bilayer membranes of a self-assembled nonionic surfactant, dodecylglyceryl itaconate, which appears as an iridescent solution as a result of Bragg reflection of visible light from the periodic lamellar planes. The large-area, ultrathin single-crystalline Au nanosheets enable the fabrication of plasmonic devices. For the first time, the property of surface plasmon polaritons on a patterned single-crystalline Au nanosheet was investigated, and a long propagation length approaching the theoretical expectation was found.

Inspired by the intriguing one-atom-thick structure and amazing physical properties of graphene, much effort has been devoted to the synthesis of other types of non-carbon two-dimensional (2D) nanomaterials and the exploration of their unique properties arising from 2D effects.¹ Compared with materials having intrinsically layered crystal structures, the controlled synthesis of 2D nanomaterials with a nonlayered structure is still underdeveloped and greatly challenging to date. Very recently, the 2D oriented attachment strategy has proven to be promising for the creation of nanosheets of nonlayered materials.² However, the 2D nanomaterials obtained through this strategy are still limited and less-reported.

Noble metals such as gold and silver are widely used in electronics, sensors, and catalysis.³ What's more, when fashioned into structures with nanosized dimensions, they enable light-involved applications in a field known as plasmonics with strongly dimension- and size-dependent characteristics.⁴ Surface plasmon polaritons (SPPs) are hybrid photon–electron waves that propagate along a metal–dielectric interface. As SPPs can be exploited to control and concentrate light below the optical diffraction limit, their application covers many areas, including subwavelength waveguides, optical antennas, surface-enhanced

spectroscopy, nanofocusing, and photovoltaics.⁵ To generate and manipulate SPPs, a rather smooth metal surface is a prerequisite to reduce losses. To date, the SPP properties of metals have been examined solely on vacuum-deposited metal films with a rather large surface roughness, which gives rise to a greatly reduced propagation length.⁶ Although novel metal plates have been synthesized widely via a wet process,⁷ the fabrication of single-crystalline metal plates with tunable thicknesses and large areas suitable for SPP processing is still far less demonstrated.

Here we report a soft 2D template-directed synthesis of ultrathin single-crystalline Au nanosheets with large areas and well-tuned thicknesses ranging from a few to several tens of nanometers. The soft template was composed of hundred-nanometer-thick water layers sandwiched by lamellar bilayer membranes of a self-assembled nonionic surfactant, dodecylglyceryl itaconate (DGI), which appears as an iridescent solution. As a result, large-area, ultrathin single-crystalline Au nanosheets with well-tuned thicknesses (5–10, 10–20, and 20–40 nm) were obtained by adjusting the concentration of the Au precursor. The investigation of SPPs on a patterned Au nanosheet with thickness of 40 nm revealed a much longer propagation length than in polycrystalline deposited films.

The synthesis of Au nanosheets was carried out in a special iridescent solution composed of lamellar bilayer membranes formed by DGI and water at low DGI concentration (2.0 wt % here). The first historical investigation of iridescent phenomena can be traced back to the pioneering works on iridescent layers, also known as Schiller layers.⁸ Similar iridescence has been also found in dilute aqueous solutions of some kinds of surfactants where lamellar bilayer membranes formed by the surfactant are separated uniformly by water with equal distances on the order of the light wavelength. Iridescent DGI solutions were first developed by Satoh and Tsujii in 1987.⁹ DGI can form lamellar bilayer membranes and generate a periodically ordered structure with water (Figure 1a). As a result of Bragg reflection of visible light on the lamellar planes, the solution presents a royal-purple color. The reflection spectrum of DGI solution (Figure 1b) shows a sharp peak at 437 nm, indicating the formation of an ordered structure with a periodic distance on the order of submicrometers throughout the whole system. According to the

Received: June 18, 2013

Published: August 13, 2013

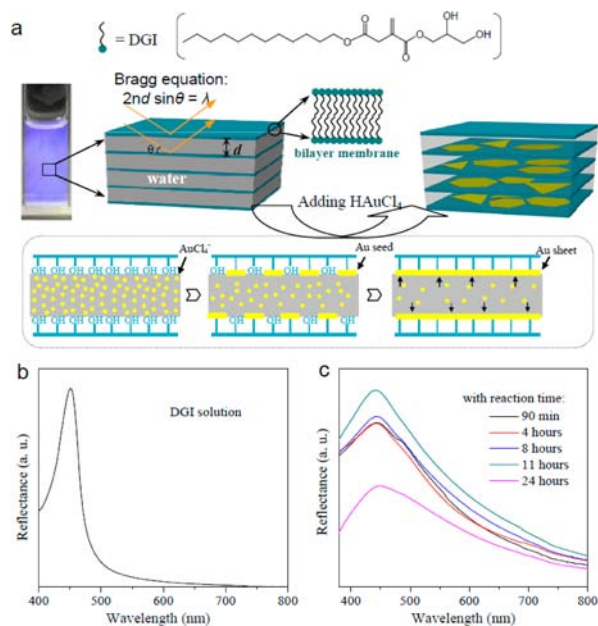


Figure 1. (a) Schematic illustration of the Au nanosheet synthesis procedure. (b) Reflection spectrum of a DGI lamellar bilayer membrane solution. (c) Reflection spectra of a DGI solution after addition of 3.5 mM HAuCl_4 recorded at various reaction times.

Bragg equation ($2nd \sin \theta = \lambda$, where n , d , θ , and λ are the refractive index of water, the periodic spacing, the angle of incidence, and the wavelength of the reflected light, respectively), the periodic spacing between adjacent DGI bilayer membranes is 166 nm.

To grow Au nanosheets, a certain amount of chloroauric acid (HAuCl_4) was introduced into the iridescent DGI solution. Reflection spectra were recorded at various reaction times. As shown in Figure 1c, the reflection peak moved to 442 nm upon addition of 3.5 mM chloroauric acid. Relative to the pristine DGI solution with no added HAuCl_4 , the reflection peak exhibited a 7 nm red shift due to a little increase in the water volume. This reflection peak corresponds to a water spacing of 168 nm. With the progress of reaction, the reflection peak remained through the whole process of Au growth, although its intensity decreased gradually. These results indicate that the periodically ordered structure of the system could be maintained during the reaction process, although there was a small negative effect on the degree of order of the system.

Control of the thickness of the Au nanosheets was carried out by adjusting the concentration of HAuCl_4 . In our experiment, Au nanosheets with well-tuned thicknesses in the range of 5–10 nm, 10–20 nm, and 20–40 nm were achieved using 2.4, 3.5, and 5.5 mM HAuCl_4 , respectively. Figure 2a shows three representative atomic force microscopy (AFM) images of Au nanosheets obtained with different concentrations and the corresponding height profiles. More precise statistical analysis of the thickness distribution was done using an optical imaging method combined with image analysis software [Figure S5 in the Supporting Information (SI)]. The results are shown in Figure 2b in the form of a histogram. It can be seen that the thickness of the Au nanosheets increased with increasing HAuCl_4 concentration. With 2.4 mM HAuCl_4 , the thickness of the Au nanosheets was 7 ± 3 nm with a narrow distribution. The thickness increased to 14 ± 4 and 30 ± 10 nm at 3.5 and 5.5 mM HAuCl_4 , respectively, and the thickness distributions became

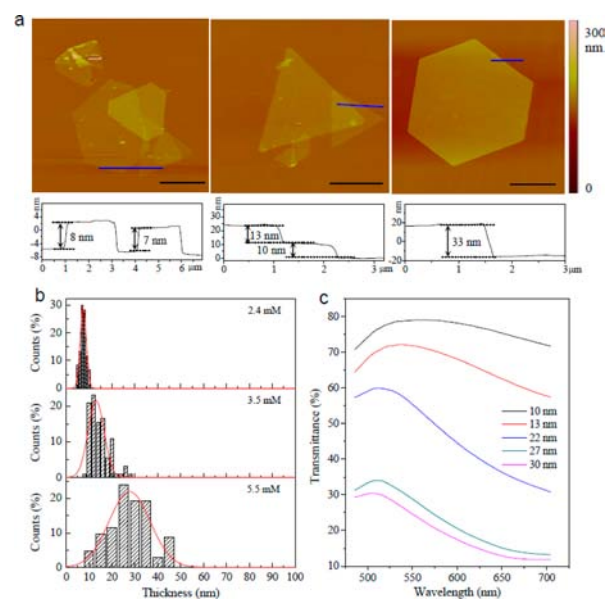


Figure 2. Control of the thickness of the Au nanosheets and their transmittance. (a) Representative AFM images of Au nanosheets obtained at different HAuCl_4 concentrations and the corresponding height profile curves (scale bar $4 \mu\text{m}$). (b) Thickness distribution histograms corresponding to different HAuCl_4 concentrations. (c) Transmittance spectra of single Au nanosheets with different thicknesses. The incident light was transmitted through the center of a calibrated Au nanosheet, and the transmitted light was recorded in a concentrated area around $2 \mu\text{m}$.

wider. Continually increasing the concentration of HAuCl_4 produced much thicker sheets and wider thickness distributions (Figure S7). As the growth of Au nanosheets was conducted in the 2D confined space of the water layer throughout the whole process, the thickest sheet that could be obtained was 100 nm because of the limit imposed by the water layer thickness.

The transmittance spectra recorded from single Au nanosheets with different thicknesses are displayed in Figure 2c. The transmittance of the Au nanosheet quickly decreased with increasing thickness. For a 10 nm thick Au nanosheet, its transparency was as high as $\sim 75\%$ over the range of 500–700 nm. These results are consistent with theoretical simulations of the transmittance of single-crystalline Au films based on the dielectric constant of bulk Au (Figure S9).¹⁰

Morphology and structure characterizations of the Au nanosheets are shown in Figure 3. Scanning electron microscopy (SEM) and transmission electron microscopy (TEM) images showed the presence of nearly all triangular and hexagonal Au sheets with micrometer-scale edge lengths, and there were few particles in the field of view (Figure 3a,b). A high-resolution TEM (HRTEM) image taken from one of the Au nanosheets revealed it to be single-crystalline with a fringe spacing of 0.24 nm (Figure 3c).^{7f,11a} The presence of the forbidden $1/3\{422\}$ reflection indicated that the surface of the Au sheet was atomically flat.^{11b} The corresponding selected-area electron diffraction (SAED) pattern (Figure 3c inset) clearly showed the single crystalline characteristic of Au, and the hexagonal diffraction spots indicated it to be highly (111)-oriented. Figure 3d shows the X-ray diffraction (XRD) pattern of Au nanosheets. The overwhelmingly strong (111) diffraction peak at $2\theta = 38.2^\circ$ and its secondary (222) diffraction peak can be clearly seen. The other two peaks, assigned to (200) and (220), are very weak relative to the (111) peak [the (200)/(111) relative diffraction

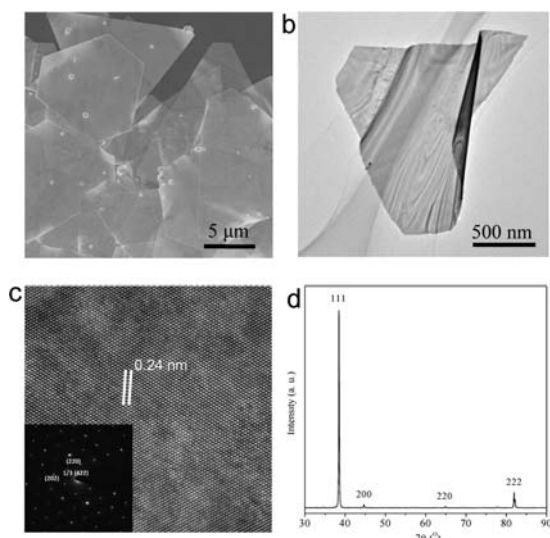


Figure 3. Morphology and structure characterization of 10–20 nm thick Au nanosheets. (a, b) Representative SEM and TEM images of Au nanosheets. (c) HRTEM image and (inset) SAED pattern of a 10 nm thick Au nanosheet. (d) XRD pattern of Au nanosheets.

intensity was 0.005, which is much lower than the Au bulk value (0.52, JCPDS no. 04-0784)].^{11b} These results reveal a preferred orientation of Au nanosheets in the (111) direction.

Our results demonstrate that the DGI lamellar bilayer membrane solution with periodically regular structure functions effectively as a soft template to induce the growth of Au nanosheets with tuned thicknesses. There are two important functions of the DGI bilayer membrane that impact the formation of Au nanosheets: reduction and 2D templating. Each DGI molecule contains two hydroxyl groups at the hydrophilic end that are in direct contact with the water layer in the system. The hydroxyl groups can function as weak reductants to reduce HAuCl_4 dispersed in the water layer to Au^0 . At the initial stage, Au nucleation is the dominant process. HAuCl_4 near the plane of lamellar bilayer membranes is first reduced by the hydroxyl groups of DGI and forms small Au seeds that adhere to the lamellar bilayer membranes. The seeds then coalesce with each other along the plane of the lamellar bilayer membranes in an oriented attachment manner, producing 2D nanosheets. During these processes, the oxidized DGI simultaneously acts as a capping agent to induce preferred growth of Au along the (111) lattice plane. It is noteworthy that the amount of DGI molecules was in excess relative to the amount of HAuCl_4 ($\text{HAuCl}_4/\text{DGI}$ molar ratio < 0.1), which means that only part of the DGI was involved in AuCl_4^- reduction. The reaction product of DGI after formation of the Au nanosheets was characterized by HPLC–MS (Figure S11), which showed that ~11% of the DGI was oxidized ultimately in the system. This ensured that the regular structure of the DGI bilayer membrane solution was well-maintained and that the 2D template could play a role through the whole process of Au growth. As the reaction proceeds, AuCl_4^- ions in the water layer diffuse toward the plane of the lamellar bilayer membranes and the growth of Au nanosheets continues. Our observation of a HAuCl_4 -concentration-dependent nanosheet thickness indicates that Ostwald ripening also occurs during the nanosheet growth process. The Au nanosheets with tuned thickness achieved in the unique DGI system reflect the function of an appropriate interlayer spacing (e.g., the thickness of water layer) on a hundred nanometer scale. Both theoretical and experimental

results have demonstrated that the viscosity of water increases in confined a 2D space in extended nanoscale.¹² In our system, the diffusion of AuCl_4^- ions in a hundred-nanometer-thick water layer is constrained to a certain extent, which decreases the Au growth rate, especially in the direction vertical to the DGI bilayer membrane. It is thus advantageous for controlling the film thickness.

The single-crystalline Au nanosheets with smooth and clean surfaces and large areas inspired us to investigate their plasmonic properties. To generate SPPs, a grating pattern with a regular periodicity width of 400 nm, a grid width of 200 nm, and a grid length of 10 μm was first fabricated on a Au nanosheet predeposited on a silicon substrate via focused-ion-beam (FIB) milling. As shown in Figure 4a, an electron beam was used to

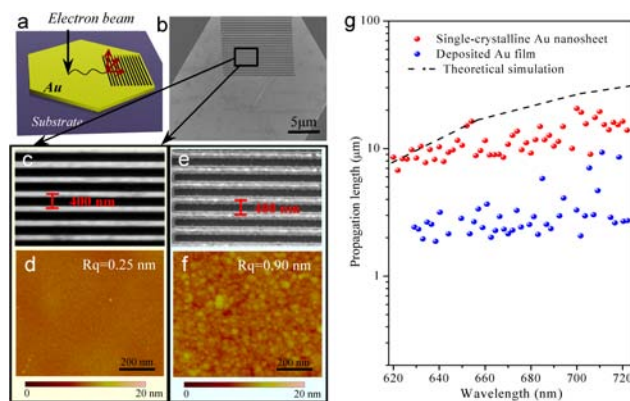


Figure 4. (a) Schematic diagram of the experimental setup for generating SPPs on a Au nanosheet. (b) SEM image of a Au nanosheet patterned with a regular grating. (c) Enlarged SEM image of the patterned grid on the Au nanosheet. (d) AFM image of the Au nanosheet recorded apart from the patterned area. (e) Enlarged SEM image of the patterned grid on a deposited Au film. (f) AFM image of the deposited Au film recorded apart from the patterned area. (g) SPP propagation lengths on the Au nanosheet and the deposited Au film.

excite SPPs of the Au nanosheet at a position micrometers away from the edge of the grafting pattern. The light outcoupled through the slit propagated along the Au surface. When the light struck the adjacent groove, it was partially scattered into the far field, and the resulting light was collected with an optical microscope. The spectra of the scattered light from all grid–groove pairs were measured, and the data were fit to an exponential decay of intensity versus distance, from which the propagation length as a function of optical wavelength was finally extracted (see the SI). Figure 4b shows an SEM image of the Au nanosheet patterned by regular grating. To demonstrate the improved plasmonic property of our single-crystalline Au nanosheet, a deposited Au film with same thickness and pattern structure as the Au nanosheet was fabricated by magnetron sputtering (Figure S10). Its SPP propagation was also measured for comparison. A significant difference in the surface flatness for the single-crystalline Au nanosheet and the deposited Au film could be observed (Figure 4c,d for the Au nanosheet and Figure 4e,f for the deposited Au film). The enlarged SEM images taken on patterned grids show that the grid structure on the single-crystalline Au nanosheet was very smooth with sharp and precise boundaries (Figure 4c), while the grid structure on deposited Au film was rather rough and the grid width seemed widened because of grain boundaries (Figure 4e). The smoothnesses of the single-crystalline Au nanosheet and deposited Au film were

further quantified with AFM (Figure 4d,f). The root-mean-square (RMS) roughness was 0.25 nm measured over an 800 nm × 800 nm region of the single-crystalline Au nanosheet, indicating an atomically smooth surface. The RMS roughness measured on the deposited Au film was as high as 0.90 nm, a representative value for most polycrystalline Au films. The SPP propagation lengths clearly show that the propagation on single-crystalline Au nanosheet was much longer than on the deposited Au film over the whole detected wavelength range, with an average 700% increase (Figure 4g). With the assumptions that the surface has zero roughness and the SPPs are damped only by Ohmic losses, the theoretically expected propagation lengths on Au were calculated, and the theoretical values were only slightly larger than the actual propagation lengths on the single-crystalline Au nanosheet. This result reveals that our single-crystalline Au nanosheets possess extremely high quality and atomically smooth surfaces. These are the longest propagation lengths generated on Au crystals reported to date. The superior plasmonic performance of the nanosheets indicates their promise for applications in plasmonic-related devices.

In conclusion, ultralarge (>100 μm²) single-crystalline Au nanosheets with well-tuned thicknesses have been successfully synthesized in a unique system with a periodically ordered structure of lamellar bilayer membranes and water. The produced Au nanosheets possess atomically smooth surfaces over large areas, which provides them superior surface plasmonic properties. The 2D template-directed growth of 2D nanomaterials in this unique system has demonstrated its effectiveness and provides a powerful alternative route for producing various 2D nanomaterials with a nonlayered structure.

■ ASSOCIATED CONTENT

📄 Supporting Information

Experimental details and additional data. This material is available free of charge via the Internet at <http://pubs.acs.org>.

■ AUTHOR INFORMATION

Corresponding Author

jjin2009@sinano.ac.cn

Author Contributions

[§]H.L.Q. and D.W. contributed equally.

Notes

The authors declare no competing financial interest.

■ ACKNOWLEDGMENTS

This work was supported by the National Natural Science Foundation of China (21273270, 21004076), the National Basic Research Program of China (2013CB933000), and the Key Development Project of the Chinese Academy of Sciences (KJZD-EW-M01-3).

■ REFERENCES

- (1) (a) Service, R. F. *Science* **2009**, *324*, 875. (b) Huang, X.; Tang, S.; Mu, X.; Dai, Y.; Chen, G.; Zhou, Z.; Ruan, F.; Yang, Z.; Zheng, N. *Nat. Nanotechnol.* **2011**, *6*, 28. (c) Butler, S. Z.; Hollen, S. M.; Cao, L.; Cui, Y.; Gupta, J. A.; Gutiérrez, H. R.; Heinz, T. F.; Hong, S. S.; Huang, J.; Ismach, A. F.; Johnston-Halperin, E.; Kuno, M.; Plashnitsa, V. V.; Robinson, R. D.; Ruoff, R. S.; Salahuddin, S.; Shan, J.; Shi, L.; Spencer, M. G.; Terrones, M.; Windl, W.; Goldberger, J. E. *ACS Nano* **2013**, *7*, 2898. (d) Huang, X.; Li, S.; Huang, Y.; Wu, S.; Zhou, X.; Li, S.; Gan, C. L.; Boey, F.; Mirkin, C. A.; Zhang, H. *Nat. Commun.* **2011**, *2*, 292.
- (2) (a) Schliehe, C.; Juarez, B. H.; Pelletier, M.; Jander, S.; Greshnykh, D.; Nagel, M.; Meyer, A.; Foerster, S.; Kornowski, A.; Klinke, C.; Weller,

H. *Science* **2010**, *329*, 550. (b) Zhang, X.; Zhang, J.; Zhao, J.; Pan, B.; Kong, M.; Chen, J.; Xie, Y. *J. Am. Chem. Soc.* **2012**, *134*, 11908.

(3) (a) Hu, L.; Kim, H. S.; Lee, J. Y.; Peumans, P.; Cui, Y. *ACS Nano* **2010**, *4*, 2955. (b) Daniel, M. C.; Astruc, D. *Chem. Rev.* **2004**, *104*, 293. (c) Jain, P. K.; Huang, X.; El-Sayed, I. H.; El-Sayed, M. A. *Acc. Chem. Res.* **2008**, *41*, 1578.

(4) (a) Millstone, J. E.; Park, S.; Shuford, K. L.; Qin, L.; Schatz, G. C.; Mirkin, C. A. *J. Am. Chem. Soc.* **2005**, *127*, 5312. (b) Hu, M.; Chen, J.; Li, Z. Y.; Au, L.; Hartland, G. V.; Li, X.; Marquez, M.; Xia, Y. *Chem. Soc. Rev.* **2006**, *35*, 1084. (c) Kim, F.; Connor, S.; Song, H.; Kuykendall, T.; Yang, P. *Angew. Chem., Int. Ed.* **2004**, *43*, 3673. (d) Chen, H.; Shao, L.; Li, Q.; Wang, J. *Chem. Soc. Rev.* **2013**, *42*, 2679. (e) Payne, C. M.; Anderson, L. J. E.; Hafner, J. H. *J. Phys. Chem. C* **2013**, *117*, 4734. (f) Wang, X.; Zhuang, J.; Peng, Q.; Li, Y. *Nature* **2005**, *437*, 121. (g) Sun, Z.; Chen, X.; Wang, L.; Zhang, G.; Jing, B. *Colloids Surf., A* **2008**, *326*, 23.

(5) (a) Bozhevolnyi, S. I.; Volkov, V. S.; Devaux, E.; Laluet, J. Y.; Ebbesen, T. W. *Nature* **2006**, *440*, 508. (b) Oulton, R. F.; Sorger, V. J.; Genov, D. A.; Pile, D. F. P.; Zhang, X. *Nat. Photonics* **2008**, *2*, 496. (c) Mühlischlegel, P.; Eisler, H. J.; Martin, O. J. F.; Hecht, B.; Pohl, D. W. *Science* **2005**, *308*, 1607. (d) Huang, J. S.; Callegar, V.; Geisler, P.; Brüning, C.; Kern, J.; Prangma, J. C.; Wu, X.; Feichtner, T.; Ziegler, J.; Weinmann, P.; Kamp, M.; Forchel, A.; Biagioni, P.; Sennhauser, U.; Hecht, B. *Nat. Commun.* **2010**, *1*, 150.

(6) (a) Nagpal, P.; Lindquist, N. C.; Oh, S. H.; Norris, D. J. *Science* **2009**, *325*, 594. (b) Wijngaarden, J. T.; Verhagen, E.; Polman, A.; Ross, C. E.; Lezec, H. J.; Atwater, H. A. *Appl. Phys. Lett.* **2006**, *88*, No. 221111.

(7) (a) Wang, L.; Chen, X.; Zhan, J.; Chai, Y.; Yang, C.; Xu, L.; Zhuang, W.; Jing, B. *J. Phys. Chem. B* **2005**, *109*, 3189. (b) Sun, X.; Dong, S.; Wang, E. *Angew. Chem.* **2004**, *116*, 6520. (c) Li, Z.; Liu, Z.; Zhang, J.; Han, B.; Du, J.; Gao, Y.; Jiang, T. *J. Phys. Chem. B* **2005**, *109*, 14445. (d) Moon, G. D.; Lim, G.; Song, J. H.; Shin, M.; Yu, T.; Lim, B.; Jeong, U. *Adv. Mater.* **2013**, *25*, 2707. (e) Kim, J.-U.; Cha, S.-H.; Shin, K.; Jho, J. Y.; Lee, J.-C. *Adv. Mater.* **2004**, *16*, 459. (f) Shankar, S. S.; Rai, A.; Ankamwar, B.; Singh, A.; Ahmad, A.; Sastry, M. *Nat. Mater.* **2004**, *3*, 482.

(8) (a) Bergmann, P.; Low-Beer, P.; Zocher, H. Z. *Phys. Chem. A* **1938**, *181*, 301. (b) Levine, S. *Trans. Faraday Soc.* **1948**, *44*, 833.

(9) Satoh, N.; Tsujii, K. *J. Phys. Chem.* **1987**, *91*, 6629.

(10) Johnson, P. B.; Christy, R. W. *Phys. Rev. B* **1972**, *6*, 4370.

(11) (a) Au, L.; Lim, B.; Colletti, P.; Jun, Y. S.; Xia, Y. *Chem.—Asian J.* **2011**, *5*, 123. (b) Li, C.; Cai, W.; Cao, B.; Sun, F.; Li, Y.; Kan, C.; Zhang, L. *Adv. Funct. Mater.* **2006**, *16*, 83.

(12) (a) Li, L.; Kazoe, Y.; Mawatari, K.; Sugii, Y.; Kitamori, T. *J. Phys. Chem. Lett.* **2012**, *3*, 2447. (b) Tsukahara, T.; Hibara, A.; Ikeda, Y.; Kitamori, T. *Angew. Chem., Int. Ed.* **2007**, *46*, 1180.